

Stability of the flow of a viscoelastic fluid past a deformable surface in the low Reynolds number limit

Paresh Chokshi and V. Kumaran

Department of Chemical Engineering, Indian Institute of Science, Bangalore 560 012, India

(Received 18 May 2007; accepted 6 September 2007; published online 17 October 2007)

The stability of the plane Couette flow of a viscoelastic fluid adjacent to a flexible surface is analyzed with the help of linear and weakly nonlinear stability theory in the limit of zero Reynolds number. The fluid is described by an Oldroyd-B model, which is parametrized by the viscosity η , the relaxation time λ , and the parameter β , which is the ratio of solvent-to-solution viscosity; $\beta = 0$ for a Maxwell fluid and $\beta = 1$ for a Newtonian fluid. The wall is modeled as an incompressible neo-Hookean solid of finite thickness and is grafted to a rigid plate at the bottom. The neo-Hookean constitutive model parametrized by the shear modulus G , augmented to include the viscous dissipation, is used for the solid medium. Previous studies for the Newtonian flow past a compliant wall predict an instability as the dimensionless shear rate $\Gamma = (\eta V / GR)$ is increased beyond the critical value Γ_c . The present analysis investigates the effect of fluid elasticity, in terms of the Weissenberg number $W = \lambda G / \eta$, on the critical value of the imposed shear rate Γ_c for various parameters. The fluid elasticity is found to increase Γ_c , indicating the stabilizing influence of the polymer addition on the viscous instability. For dilute polymeric solutions with $\beta \geq 0.5$, the flow is stable when the Weissenberg number is increased beyond a maximum value W_{\max} , and W_{\max} increases proportional to the ratio of solid-to-fluid thickness H . For concentrated polymer solutions and melts with $\beta < 0.5$, the flow becomes unstable when the strain rate increases beyond a critical value for any large Weissenberg number. The weakly nonlinear analysis reveals that the bifurcation of the linear instability is subcritical when there is no dissipation in the solid. The nature of bifurcation, however, changes to supercritical when the viscous effects in the solid are taken into account and the relative solid viscosity η_r is large such that $\sqrt{\eta_r} / H > 1$. The equilibrium amplitude and the threshold strain energy for the solid have been calculated, and the effect of parameters H , β , η_r , and interfacial tension on these quantities is analyzed. © 2007 American Institute of Physics. [DOI: 10.1063/1.2798069]

I. INTRODUCTION

Recently, there has been a renewed interest in low Reynolds number flows due to their importance in microfluidic applications. The rate of transport of mass and heat in such systems can be enhanced if the laminar nature can be rendered unstable to generate a well-mixed flow. Making the surface flexible is a potential candidate, as the wall flexibility is known to induce an instability by surface oscillations. Deformable surfaces have been an object of research for many years since the pioneering experiments of Kramer, who found that the compliant nature of the surface is instrumental in delaying the onset of transition to turbulence in the boundary layer flows.¹ Many theoretical and experimental studies have been carried out in various flow regimes and diverse flow geometries to exploit the benefits of the oscillatory waves generated by the elastic surface in order to serve the numerous technological applications. For Newtonian flow through a gel-walled tube, the experiments by Krindel and Silberberg² indicated the transition Reynolds number to be much lower than 2100, the corresponding value for the rigid tube. Moreover, the transition Reynolds number was influenced by the elasticity of the surface in addition to the fluid properties, indicating that the wall dynamics plays a significant role in transition. Motivated by this observation, exten-

sive studies of the linear stability analysis of the Newtonian fluid flow in tubes and channels bounded by gel walls have been carried out.³⁻⁷

The relevant studies for the Newtonian fluid will be reviewed first. Kumaran *et al.*³ analyzed the linear stability of a shear flow past a flexible surface in the low Reynolds number regime, where $Re \equiv (\rho VR / \eta) \ll 1$, and $(V\eta / GR) \sim 1$. Here, V is the velocity of the top plate, ρ is the density of the fluid, η is the viscosity of the fluid, R is the channel width, and G is the shear modulus of the gel wall. The deformable wall was modeled as an incompressible linear viscoelastic solid. The authors observed that the coupling between the fluid flow and the wall dynamics renders the flow unstable even in the absence of fluid inertia.³ The instability, which occurs when the imposed shear rate, $\Gamma = V\eta / (GR)$, exceeds a certain critical value Γ_c , is driven by a discontinuity in the strain rate across the fluid-gel interface. The destabilizing mechanism is the transfer of energy from the mean flow to the fluctuations due to the shear work done by the mean flow at the interface. A similar analysis of viscous instability in flow through a flexible tube was performed by Kumaran.⁴

For a plane Couette flow, the strain in the solid is $O(1)$ when the viscous stresses in the fluid are comparable to the elastic stresses in the solid. For such a case, the classical

linear elasticity theory, which is valid for small strain, is insufficient and it is necessary to incorporate the finite strain terms in the constitutive relation for the elastic solid. This argument led Gkanis and Kumar⁸ to analyze the viscous instability using the more appropriate neo-Hookean elastic model, which is a generalization of the classical linear constitutive equation, valid for the finite displacement gradients.⁹ The viscous flow stability problem for the neo-Hookean constitutive model exhibits a nonzero first normal-stress difference in the base-state under simple shear, which was absent in the analysis of Kumaran *et al.*³ The linear stability analysis of Gkanis and Kumar examined the role of finite deformations in the viscous instability, and it was observed that the discontinuity in the first normal-stress difference across the interface results in a shortwave instability in the absence of inertia and interfacial tension. The neo-Hookean solid results in smaller values of the critical shear rate Γ_c and larger values of the critical wavenumber α_c , compared to the linear elastic model.⁸ The difference, however, diminishes as the ratio of solid-to-fluid thickness H increases, and becomes insignificant for $H \geq 10$. The analysis was extended to the pressure-driven creeping flow in a channel bounded by walls modeled as a neo-Hookean solid.¹⁰

The experimental confirmation of the viscous instability was reported by Kumaran and Muralikrishnan,¹¹ who used silicone oil of thickness 300–1000 μm on a polyacrylamide gel of thickness about 4.5 mm in a parallel-plate rheometer. They observed a sharp increase in the apparent viscosity (calculated by assuming the flow to be laminar) when the imposed shear rate exceeds a certain critical value. The experimental value of critical shear rate required for the onset of instability was found to be in good agreement with the theoretical predictions of Ref. 3 for a wide range of gel thicknesses and elastic moduli.^{11,12} As the gel thickness H was greater than 5 in these experiments, the results for the neo-Hookean model are in agreement with those for the linear elastic model.

For the viscoelastic fluid, a considerable amount of work has been done to study the stability of a shear flow past a rigid surface, to investigate the nature of the eigenspectrum for the growth rate.^{13–15} In most studies, the viscoelastic fluid is described either by the *upper convected Maxwell* (UCM) model or the *Oldroyd-B* model, wherein the polymer chains are treated as the elastic dumbbells. For the flexible surface, Shankar and Kumar¹⁶ have studied the linear stability of the UCM fluid in plane Couette flow in the creeping flow limit. The flexible wall is described by an incompressible linear viscoelastic solid model. The analysis predicts an unstable viscous mode when the dimensionless strain rate $\Gamma = V\eta/(GR)$ exceeds a certain critical value. Their analysis recovers the stable modes for UCM fluid flow past a rigid surface reported by Gorodtsov and Leonov¹³ (the GL modes) as well as the unstable viscous mode for Newtonian fluid flow past gel of Kumaran, Fredrickson, and Pincus³ (the KFP mode). The analysis of Shankar and Kumar shows that the wall elasticity has a destabilizing effect on one of the two discrete GL modes, whereas the fluid elasticity has a stabilizing influence on the unstable KFP mode for the Newtonian fluid.¹⁶ Since the UCM model ignores the viscous contribu-

tion due to the solvent, the model is suitable for the polymer melt. In the present study, we consider a more general Oldroyd-B fluid that takes into account the solvent contribution, and hence represents the polymer solution of varying concentration. Further, we use the more realistic neo-Hookean model to describe the dynamics in the solid. Recently, Chokshi and Kumaran¹⁷ analyzed the linear stability of an Oldroyd-B fluid flow past a linear viscoelastic solid. They found, for the dilute polymeric solutions, an unstable shortwave mode that is absent for the UCM fluid.¹⁶ This shortwave instability is in addition to the finite wavenumber KFP mode modified for the viscoelastic fluid. The present analysis, which uses the neo-Hookean model, shows that the nature of shortwave instability is greatly influenced by the finite deformation terms ignored in the linear elastic model.

The above discussed studies were restricted to the linear stability of the base flow, which determines whether the flow is stable or unstable to infinitesimal disturbances, but does not provide information about the evolution of the flow after transition. In the present analysis, we use a finite-amplitude weakly nonlinear stability analysis to determine the nature of bifurcation. The weakly nonlinear analysis is based on an equation for the disturbance amplitude of the form $dA_1/dt = s^{(0)}A_1 + s^{(1)}A_1^3 + \dots$. Here $s^{(0)}$ is the linear growth rate, and $s^{(1)}$ is called the first Landau constant. The bifurcation is supercritical if $s^{(1)}$ is negative, indicating that the saturation amplitude of the disturbance increases continuously from zero as the scaled strain rate is increased above its critical value. The bifurcation is subcritical if $s^{(1)}$ is positive, indicating that perturbations that are stable in the linear analysis become unstable to perturbations with amplitude larger than $(|s^{(0)}|/s^{(1)})^{1/2}$. The weakly nonlinear theory has been developed based on the pioneering works of Stuart¹⁸ and Watson,¹⁹ which treat the nonlinearities using an amplitude expansion. This involves the assumption that the higher harmonics are generated by the nonlinear interactions of the fundamental mode at the onset of instability. For a flow past a flexible surface, the nonlinearities appear in the boundary conditions applied at the fluid-wall interface, in addition to the nonlinearities present in the governing equations. A weakly nonlinear analysis for the unstable viscous mode in the Newtonian flow was performed by Shankar and Kumaran,²⁰ using the linear viscoelastic constitutive equation for the flexible solid. The authors found the bifurcation to be subcritical for a wide range of parameters. The recent experiments conducted with a layer of viscous fluid on the cross-linked polydimethylsiloxane (PDMS) gel in a parallel-plate rheometer confirmed the subcritical nature of the viscous instability.²¹

We carry out the linear and weakly nonlinear stability analyses of an Oldroyd-B fluid flow past a neo-Hookean viscoelastic solid. The neo-Hookean model, which describes the rubberlike materials, is supplemented with the viscous effects likely to be present in the polymeric gel-like solids. The viscous stresses are modeled using an upper convected Maxwell model. The rest of this paper is organized as follows. The fluid and solid governing equations in Eulerian framework are provided in Sec. II. The weakly nonlinear stability analysis is described briefly in Sec. III. The results of the

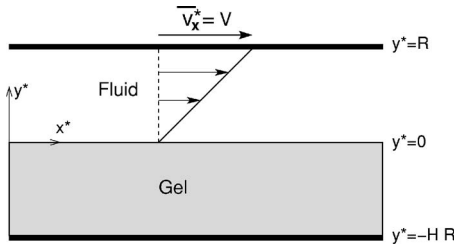


FIG. 1. Schematic diagram of plane Couette flow over a flexible surface showing the dimensional coordinate system.

linear and the weakly nonlinear analyses are presented and discussed in Sec. IV. The important conclusions are summarized in Sec. V.

II. PROBLEM FORMULATION

The base flow configuration and the coordinate system are shown in Fig. 1. The system consists of an incompressible viscoelastic fluid of density ρ and viscosity η occupying the domain $0 < y^* < R$. Here, the superscript $*$ for the y coordinate implies that it is dimensional; the scaled y coordinate is defined as $y = (y^*/R)$. The fluid is supported on an incompressible deformable solid medium of shear modulus G , density ρ , viscosity η_s , and thickness HR . The top plate at $y^* = R$ is set moving in the x direction with velocity V , where as the bottom rigid wall at $y^* = -HR$ is held stationary. In the nondimensionalization scheme used here, the distance is scaled with R , time with η/G , velocity with GR/η , and pressure and stresses in fluid as well as in wall are scaled with G . The scaled fluid continuity and momentum balance equations in the absence of inertia are as follows:

$$\nabla \cdot \mathbf{v} = 0, \quad (1)$$

$$\nabla \cdot \boldsymbol{\tau} = 0, \quad (2)$$

where \mathbf{v} denotes the fluid velocity field. For the viscoelastic fluid modeled as an Oldroyd-B fluid, the total stress tensor $\boldsymbol{\tau}$ consists of the isotropic fluid pressure p_f , the viscous stress due to the solvent ($\boldsymbol{\tau}^s$), and the polymeric stress ($\boldsymbol{\tau}^p$):

$$\boldsymbol{\tau} = -p_f \mathbf{I} + \boldsymbol{\tau}^s + \boldsymbol{\tau}^p, \quad (3)$$

where \mathbf{I} is the identity tensor. The dimensionless viscous stress arising due to the solvent viscosity (η_s) is of the form

$$\boldsymbol{\tau}^s = \beta [\nabla \mathbf{v} + (\nabla \mathbf{v})^T], \quad (4)$$

where the superscript T indicates the transpose. The parameter $\beta = \eta_s/\eta$ is introduced to represent the solvent contribution to the solution viscosity η , where $\eta = \eta_s + \eta_p$. The polymer contribution is given by $(1 - \beta) = \eta_p/\eta$.

The polymeric stress $\boldsymbol{\tau}^p$ is expressed in terms of the polymer chain conformation tensor \mathbf{c} , which is given by the single relaxation time constitutive model,

$$\mathcal{D}_t^* \mathbf{c} = - \frac{(\mathbf{c} - \mathbf{c}^{*eq})}{\lambda}. \quad (5)$$

The material time derivative $\mathcal{D}_t^* \mathbf{c}$ is the upper convected time derivative of \mathbf{c} defined as

$$\mathcal{D}_t^* \mathbf{c} = \partial_t^* \mathbf{c} + \mathbf{v}^* \cdot \nabla \mathbf{c} - \mathbf{c}^* \cdot (\nabla \mathbf{v}^*) - (\nabla \mathbf{v}^*)^T \cdot \mathbf{c}^*. \quad (6)$$

Under no-flow conditions, the equilibrium chain conformation is $\mathbf{c}^{*eq} = (k_B T/H) \delta_{ij}$, where H is the spring constant and $k_B T$ is the thermal energy. The polymeric stress, which is proportional to the departure of the conformation tensor from its equilibrium value, is given by the expression

$$\boldsymbol{\tau}^{*p} = \frac{\eta_p H}{\lambda k_B T} (\mathbf{c}^* - \mathbf{c}^{*eq}). \quad (7)$$

We nondimensionalize the conformation tensor \mathbf{c}^* by $(k_B T/H)$, $\boldsymbol{\tau}^{*p}$ with G and time with η/G , to obtain the following constitutive model:

$$\mathcal{D}_t \mathbf{c} = \frac{(\mathbf{c} - \mathbf{I})}{W}, \quad (8)$$

$$\boldsymbol{\tau}^p = (1 - \beta) \frac{(\mathbf{c} - \mathbf{I})}{W}, \quad (9)$$

where the Weissenberg number $W = (\lambda G/\eta)$ is the dimensionless relaxation time of the Oldroyd-B fluid.

Substituting the expressions of $\boldsymbol{\tau}^s$ and $\boldsymbol{\tau}^p$ in the momentum conservation equation (2), we obtain

$$0 = -\nabla p_f + \beta \nabla^2 \mathbf{v} + \nabla \cdot \boldsymbol{\tau}^p. \quad (10)$$

The momentum conservation equation for the Newtonian fluid is recovered in the limit $W \rightarrow 0$ as well as for $\beta = 1$, and the governing equation for the upper convected Maxwell (UCM) fluid is obtained for $\beta = 0$.

The deformable wall is modeled as an incompressible neo-Hookean viscoelastic solid continuum wherein the neo-Hookean constitutive model is augmented with a viscous stresses to account for the viscous dissipation in the solid. The neo-Hookean elastic solid model has been used in the previous studies of linear stability analyses of a Newtonian flow.^{8,10} In the Eulerian description, the dynamics of the elastic solid is described by a displacement field \mathbf{u} , given by the displacement of a particle from the initial reference configuration, \mathbf{X} , to a configuration \mathbf{x} at any time t as

$$\mathbf{x} = \mathbf{X} + \mathbf{u}(\mathbf{x}, t). \quad (11)$$

The deformation tensor in spatial configuration is given by

$$\mathbf{f} = \frac{\partial \mathbf{X}}{\partial \mathbf{x}} = (\mathbf{I} - \nabla \mathbf{u}). \quad (12)$$

The mass conservation condition for an incompressible solid is given by either

$$\det \mathbf{f} = 1 \quad (13)$$

or

$$\nabla \cdot \mathbf{v}^g = 0, \quad (14)$$

where \det indicates the determinant and \mathbf{v}^g is the dimensionless Eulerian velocity field in the wall medium given by

$$\mathbf{v}^g = \partial_t \mathbf{u} + \mathbf{v}^g \cdot \nabla \mathbf{u}. \quad (15)$$

The dimensionless momentum balance equation, in the absence of inertia, is

$$\nabla \cdot \boldsymbol{\sigma} = 0. \quad (16)$$

The total stress tensor in the solid, scaled by the shear modulus G , is

$$\boldsymbol{\sigma} = -p_g \mathbf{I} + 2\mathbf{e} + \boldsymbol{\sigma}^V, \quad (17)$$

where p_g is the isotropic pressure, the elastic contribution $\boldsymbol{\sigma}^E$ is proportional to the strain \mathbf{e} , and the viscous contribution $\boldsymbol{\sigma}^V$ is proportional to the strain rate. The strain tensor in the neo-Hookean elastic solid is given by⁹

$$\mathbf{e} = \frac{1}{2}(\mathbf{I} - \mathbf{f}^T \cdot \mathbf{f}) \quad (18)$$

or

$$e_{ij} = \frac{1}{2} \left(\frac{\partial u_i}{\partial x_j} + \frac{\partial u_j}{\partial x_i} - \frac{\partial u_k}{\partial x_i} \frac{\partial u_k}{\partial x_j} \right). \quad (19)$$

The viscous stress tensor is described by a single relaxation time upper convective Maxwell model,

$$\boldsymbol{\sigma}^V + \text{De}[\partial_t \boldsymbol{\sigma}^V + \mathbf{v}^g \cdot \nabla \boldsymbol{\sigma}^V - \boldsymbol{\sigma}^V \cdot (\nabla \mathbf{v}^g) - (\nabla \mathbf{v}^g)^T \cdot \boldsymbol{\sigma}^V] = 2\eta_r \dot{\mathbf{e}}, \quad (20)$$

where the Deborah number is the relaxation time (λ_g) scaled with the flow time scale, $\text{De} = \lambda_g G / \eta$ and $\eta_r = \eta_g / \eta$, the ratio of the wall viscosity to the fluid viscosity. The strain rate tensor $\dot{\mathbf{e}}$ for the neo-Hookean solid is given by⁹

$$\dot{\mathbf{e}} = \frac{1}{2}[(\nabla \mathbf{v}^g)^T + \nabla \mathbf{v}^g] - [\mathbf{e} \cdot (\nabla \mathbf{v}^g)^T + \nabla \mathbf{v}^g \cdot \mathbf{e}] \quad (21)$$

or

$$\dot{e}_{ij} = \frac{1}{2} \left(\frac{\partial v_i^g}{\partial x_j} + \frac{\partial v_j^g}{\partial x_i} \right) - \left(e_{ik} \frac{\partial v_k^g}{\partial x_j} + \frac{\partial v_k^g}{\partial x_i} e_{kj} \right). \quad (22)$$

A model similar to above has been used by Phan-Thien²² to describe a class of soft viscoelastic materials that includes bread dough and some biological tissues. This model incorporates both the neo-Hookean rubberlike response and the viscoelastic response modeled by a Maxwell-type equation. In the limit $\text{De} \rightarrow 0$, the viscous stress is given by the simple expression of Newton's law. Even for a finite Deborah number, the nonlinear terms in the upper convected time derivative part in the expression (20) are identically zero for the linear stability problem, because $\mathbf{v}^g = \boldsymbol{\sigma}^V = 0$ for the base state considered in the present study. Furthermore, as $\boldsymbol{\sigma}^V = 0$ for zero viscosity in the wall, the neo-Hookean elastic model is recovered in the limit $\eta_r \rightarrow 0$. For a major part of the present analysis, the value of η_r is kept zero, thus the stability behavior is studied for the neo-Hookean elastic solid. Later, the effect of wall viscosity on the critical shear rate is analyzed for a set of parameters using the above-described constitutive model for the viscous stresses.

For the steady-state base flow shown in Fig. 1, the fluid velocity, the wall displacement, and velocity fields are given as

$$\bar{\mathbf{v}} = (\Gamma y, 0, 0), \quad \bar{\mathbf{u}} = [\Gamma(y+H), 0, 0], \quad \bar{\mathbf{v}}^g = (0, 0, 0), \quad (23)$$

where $\Gamma = V\eta/(GR)$ is the dimensionless velocity of the top plate and hence is the shear rate for fluid. The base state stresses in the fluid and wall medium are

$$\bar{\tau}_{xx} = -\bar{p}_f + 2(1-\beta)W\Gamma^2, \quad \bar{\tau}_{xy} = \Gamma, \quad \bar{\tau}_{yy} = -\bar{p}_f, \quad (24)$$

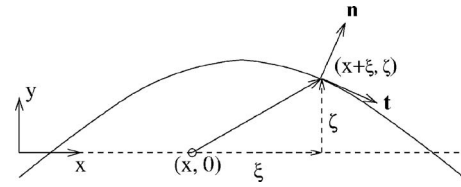


FIG. 2. Schematic illustrating the perturbed fluid-solid interface.

$$\bar{\sigma}_{xx} = -\bar{p}_g, \quad \bar{\sigma}_{xy} = \Gamma, \quad \bar{\sigma}_{yy} = -\bar{p}_g - \Gamma^2, \quad (25)$$

$$\bar{p}_f = \bar{p}_g = \text{const.}$$

In addition to the no-slip conditions, $\bar{v}_x = \Gamma$ at $y=1$ and zero displacement for a wall fixed at $y=-H$, the base state also satisfies the normal and tangential velocity and stress continuity conditions at the fluid-wall interface, which, for the mean flow, is flat at $y=0$. The nonzero value of the first normal-stress difference $\bar{\sigma}_{xx} - \bar{\sigma}_{yy} = \Gamma^2$ for the elastic solid is a consequence of the neo-Hookean constitutive model, which retains the terms quadratic in displacement gradient Γ . This additional stress, which was absent in the linear viscoelastic solid analyses,^{3,16,17} affects the linear stability of the base state, especially when the shear rate $\Gamma > 1$, as found by Gkanis and Kumar.⁸ The viscoelastic fluid also exhibits the nonzero first normal-stress difference $\bar{\tau}_{xx} - \bar{\tau}_{yy} = 2(1-\beta)W\Gamma^2$. This additional stress vanishes in the limit of Newtonian fluid ($\beta=1$ or $W \rightarrow 0$).

III. WEAKLY NONLINEAR ANALYSIS

In addition to the fluid and the solid governing equations, the nonlinearities also arise from the fluid-wall interface boundary conditions.^{20,23} While the interface in the undisturbed flow is flat at $y=0$, its position in the perturbed flow is different and has to be obtained as a part of the solution. As illustrated schematically in Fig. 2, a material point $(x, 0)$ on the undisturbed interface moves to a position $(x+\xi, \zeta)$ due to the perturbations, where ξ and ζ are Lagrangian displacement of the material point at the interface. The matching conditions at the perturbed interface are

$$(\mathbf{t} \cdot \mathbf{v})|_{x+\xi, \zeta} = (\mathbf{t} \cdot \mathbf{v}^g)|_{x+\xi, \zeta}, \quad (26)$$

$$(\mathbf{n} \cdot \mathbf{v})|_{x+\xi, \zeta} = (\mathbf{n} \cdot \mathbf{v}^g)|_{x+\xi, \zeta}, \quad (27)$$

$$(\mathbf{t} \cdot \boldsymbol{\tau} \cdot \mathbf{n})|_{x+\xi, \zeta} = (\mathbf{t} \cdot \boldsymbol{\sigma} \cdot \mathbf{n})|_{x+\xi, \zeta}, \quad (28)$$

$$(\mathbf{n} \cdot \boldsymbol{\tau} \cdot \mathbf{n})|_{x+\xi, \zeta} = (\mathbf{n} \cdot \boldsymbol{\sigma} \cdot \mathbf{n})|_{x+\xi, \zeta} + T(\nabla_s \cdot \mathbf{n})|_{x+\xi, \zeta}. \quad (29)$$

Here, the scaled interfacial tension $T = \gamma/GR$, where γ is the dimensional surface tension and ∇_s is the gradient along the interface. \mathbf{n} and \mathbf{t} are the unit vectors normal and tangent to the perturbed interface (see Fig. 2). Denoting F and G as a dynamical variable in the fluid and wall, respectively, the interface conditions have the following generic form:

$$F|_{x+\xi, \zeta} = G|_{x+\xi, \zeta}. \quad (30)$$

In a weakly nonlinear analysis, the amplitudes of the perturbation quantities are assumed to be small but finite. Consequently, the quantities at the perturbed interface $(x+\xi, \zeta)$ can

be approximated as a Taylor expansion about their values at the unperturbed interface $(x, 0)$. Thus, the generic expression of the interface conditions, Eq. (30), becomes

$$\begin{aligned} & [F]_0 + [\partial_x F]_0 \xi + [\partial_y F]_0 \zeta + \frac{1}{2} [\partial_x^2 F]_0 \xi^2 + \frac{1}{2} [\partial_y^2 F]_0 \zeta^2 \\ & + [\partial_x \partial_y F]_0 \xi \zeta + \dots \\ & = [G]_0 + [\partial_x G]_0 \xi + [\partial_y G]_0 \zeta + \frac{1}{2} [\partial_x^2 G]_0 \xi^2 + \frac{1}{2} [\partial_y^2 G]_0 \zeta^2 \\ & + [\partial_x \partial_y G]_0 \xi \zeta + \dots, \end{aligned} \tag{31}$$

where $[\dots]_0$ denote quantities evaluated at the unperturbed interface $(y=0)$. Here ξ and ζ are obtained using the following Taylor expansions:

$$\begin{aligned} \xi & \equiv u_x(x + \xi, \zeta, t) \\ & = [u_x]_0 + [\partial_x u_x]_0 \xi + [\partial_y u_x]_0 \zeta + \frac{1}{2} [\partial_x^2 u_x]_0 \xi^2 + \frac{1}{2} [\partial_y^2 u_x]_0 \zeta^2 \\ & + [\partial_x \partial_y u_x]_0 \xi \zeta + \dots, \end{aligned} \tag{32}$$

$$\begin{aligned} \zeta & \equiv u_y(x + \xi, \zeta, t) \\ & = [u_y]_0 + [\partial_x u_y]_0 \xi + [\partial_y u_y]_0 \zeta + \frac{1}{2} [\partial_x^2 u_y]_0 \xi^2 + \frac{1}{2} [\partial_y^2 u_y]_0 \zeta^2 \\ & + [\partial_x \partial_y u_y]_0 \xi \zeta + \dots. \end{aligned} \tag{33}$$

The expressions for ξ and ζ , in terms of displacement components u_x and u_y and their derivatives evaluated at $y=0$, can be obtained from the above expansions up to the desired order of wall perturbation amplitude.

The theory of weakly nonlinear analysis is briefly discussed next. A two-dimensional perturbation of small but finite amplitude $A_1(\tau)$ with axial wavenumber α and wavespeed c (frequency $\omega = -\alpha c$) is superimposed on the base state at the critical condition. Here, τ is the slow time scale, which will be defined later. Using the definition $E(x, t) = \exp[i(\alpha x + \omega t)]$ for convenience, a general field ϕ is expanded in a harmonic-amplitude series as follows:^{18,19}

$$\begin{aligned} \phi(x, y, t) & = \bar{\phi}(y) + \sum_{k=0}^{\infty} \sum_{n=k, n \neq 0}^{\infty} [A_1(\tau)]^n [E^k \bar{\phi}^{(k,n)}(y) \\ & + E^{-k} \bar{\phi}^{(k,n)\dagger}(y)], \end{aligned} \tag{34}$$

where the overbar represents the base flow quantity, the superscript \dagger denotes the complex conjugate, and $\phi = [\mathbf{v}, p_f, \mathbf{u}, p_g]$. Here and in what follows, k denotes the harmonic index and n denotes the asymptotic order. The perturbation amplitude $A_1(\tau)$, which varies on the slow time scale τ , is a small parameter and is written as $A_1(\tau) = \epsilon A(\tau)$, where ϵ is the small parameter in the expansion and $A(\tau) \sim O(1)$. It should be noted that $A_1(\tau)$ is a real quantity, since the temporal oscillations are included in $E(x, t)$.

In the vicinity of the point of critical stability, the disturbance amplitude is assumed to satisfy the following equation known as the Landau equation:

$$A_1(\tau)^{-1} d_t A_1(\tau) = s_r^{(0)} + A_1(\tau)^2 s_r^{(1)} + \dots, \tag{35}$$

where the constant $s_r^{(0)}$ is the real part of the linear growth rate $s^{(0)}$, which emerges as an eigenvalue from the classical linearized stability analysis. The linear growth rate is related to the wavespeed as $s^{(0)} = -i\alpha c$. The constant $s_r^{(1)}$ is the real

part of the first Landau constant $s^{(1)}$. If the flow is neutrally stable to infinitesimal disturbance, that is, $s_r^{(0)} = 0$, then the sign of $s_r^{(1)}$ determines the growth or decay of a weak disturbance. In the neighborhood of neutral stability such that $(\Gamma - \Gamma_c) \ll 1$, the linear growth rate can be expressed as $s_r^{(0)} = (\Gamma - \Gamma_c)(ds_r^{(0)}/d\Gamma)$. If $s_r^{(1)}$ is $O(1)$, then the second term on the right-hand side of Eq. (35) is $O(\epsilon^2)$, and the balance with the first term is achieved if $(\Gamma - \Gamma_c)(ds_r^{(0)}/d\Gamma) \sim \epsilon^2$. For definiteness, let $(\Gamma - \Gamma_c) = \Gamma_2 \epsilon^2$, where Γ_2 is $O(1)$. In order to establish a balance between the right and left sides of Eq. (35), we introduce the slow time scale τ such that the time derivative d_t is written as $d_t \rightarrow d_t + \epsilon^2 d_\tau$. Hence, there exist multiple time scales in the system: a fast time scale (t) corresponding to the inverse of the frequency of oscillations, and a slow time scale (τ) corresponding to the rate of growth or decay of the disturbance amplitude. Since $A_1(\tau)$ is independent of the fast time scale t , the scaled dynamical equation for the amplitude becomes

$$A(\tau)^{-1} d_\tau A(\tau) = \Gamma_2 \frac{ds_r^{(0)}}{d\Gamma} + A(\tau)^2 s_r^{(1)} + \dots. \tag{36}$$

The imaginary part of the first Landau constant provides the correction of the perturbation frequency due to the nonlinear interactions.

The objective of the rest of the analysis is to determine the first Landau constant $s^{(1)}$, which in turn determines whether the nature of viscous instability is supercritical ($s_r^{(1)} < 0$) or subcritical ($s_r^{(1)} > 0$). Upon expanding all the dynamical quantities in the harmonic-amplitude series, as shown in (34), and extracting the governing equations at various orders, the inhomogeneous terms appear in the fluid and the wall governing equations and the interface conditions. In general, the problem at order (k, n) contains inhomogeneous terms of order (j, m) , where $m < n$ and $j + m \leq k + n$. In the hierarchy of problems at various orders, the Landau constant $s^{(1)}$ first appears in the problem with $k=1$ and $n=3$. Therefore, in the weakly nonlinear analysis, where the objective is to calculate only the first Landau constant, only few selected problems at orders $(1,1)$, $(0,2)$, $(2,2)$, and $(1,3)$ need to be solved, necessarily in that order. The $(1,1)$ problem is the linear stability analysis, which provides the critical point around which the harmonic-amplitude expansion is carried out; the $(0,2)$ problem provides $O(A_1^2)$ correction to the mean flow, often termed the base flow distortion; the $(2,2)$ problem is the first harmonic of the fundamental mode which manifests at order A_1^2 ; and the $(1,3)$ problem is the nonlinear correction to the least stable fundamental mode, at which order the Landau equation (35) is recovered. For details of the solution procedure, the readers are referred to Refs. 24–26.

IV. RESULTS AND DISCUSSIONS

A. Linear stability analysis

1. Neo-Hookean elastic solid

In this section, we discuss the results of the linear stability analysis for the neo-Hookean solid with the relative viscosity of solid set equal to zero, $\eta_r = 0$. The transition param-

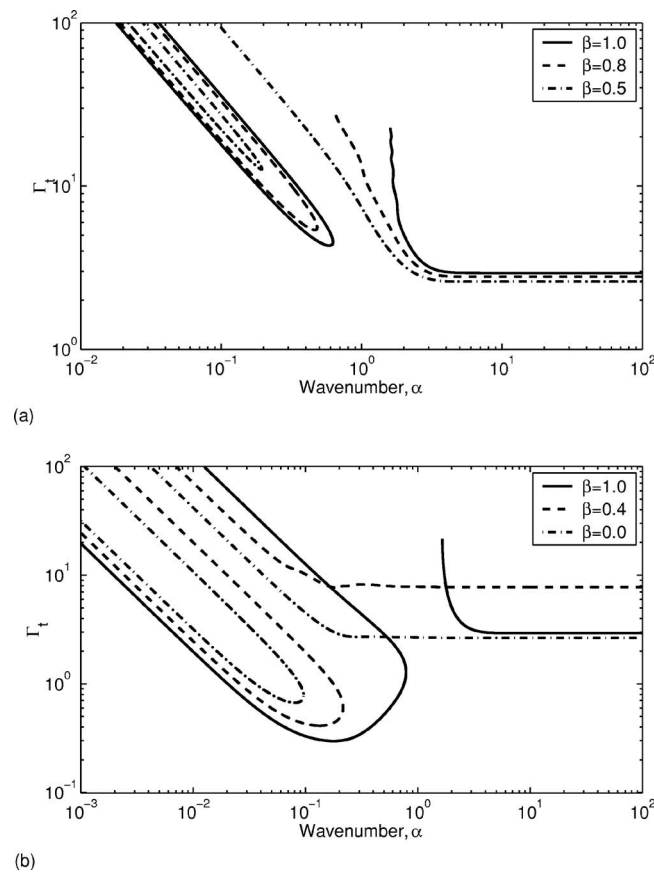


FIG. 3. Neutral stability curve showing the transition shear rate Γ_t as a function of wavenumber α for (a) $H=1$, $W=0.15$; (b) $H=10$, $W=5$. For both plots, η_r and T are kept zero.

eter Γ_t , determined by setting the leading-order growth rate $s_r^{(0)}=0$, depends on the wavenumber α , the solid-to-fluid thickness ratio H , the fluid Weissenberg number $W=\lambda G/\eta$, the polymer concentration parameter $\beta=\eta_s/\eta$, and the interfacial tension $T=\gamma/GR$. Figure 3 shows typical neutral stability diagrams for different sets of parameters. The plots for $\beta=1$ correspond to the Newtonian fluid analyzed by Ref. 8. For a neo-Hookean solid, there exist two classes of modes, viz., the finite wavenumber mode, for which Γ_t is minimum for a finite wavenumber, and the shortwave mode, characterized by a plateau in Γ_t in the limit of large wavenumber. For a neo-Hookean solid, the shortwave instability is due to a jump in the first normal-stress difference across the fluid-solid interface that is absent for the linear elastic solid.⁸ Such a jump is known to excite a shortwave instability at the interface between two flowing viscoelastic fluid layers in the absence of interfacial tension and inertia.¹⁴ For $H=1$, Fig. 3(a) shows that the value of Γ_t for the shortwave instability is lower than the value of Γ_t observed for the finite wavenumber instability. Thus, the critical value Γ_c lies in the high wavenumber region. The shortwave modes are upstream traveling waves with negative wavespeed, whereas the finite wavenumber modes are downstream traveling waves. While Γ_t for the shortwave instability is independent of the solid thickness H , the value of Γ_t for the finite wavenumber instability decreases upon increasing H . Hence, for $H=10$, the

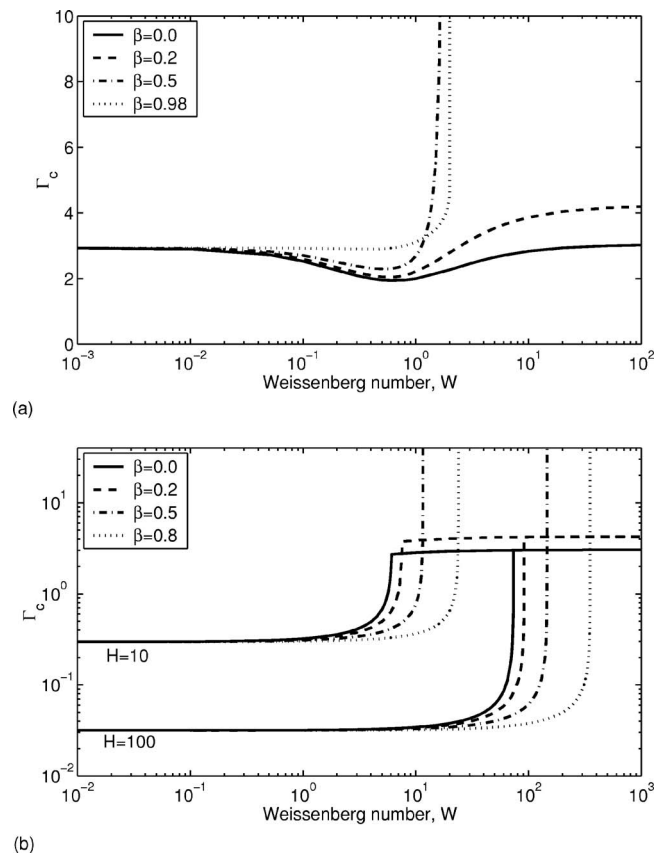


FIG. 4. Variation of the critical shear rate Γ_c with Weissenberg number: (a) $H=1$. The instability in thin solids is driven by the shortwave mode; (b) $H=10$ and 100. The plateau in Γ_c represents the highly elastic shortwave mode. For both plots, η_r and T are kept zero.

critical point (α_c, Γ_c) lies on the finite wavenumber part of the neutral stability diagram, as shown in Fig. 3(b).

For relatively thin solids with $H=1$, for which case the shortwave mode is the critical mode of instability, Fig. 4(a) shows the variation of the critical value of the imposed shear rate Γ_c with Weissenberg number for different values of β . For $\beta \geq 0.5$, which represents the dilute polymeric solutions, Γ_c diverges at Weissenberg number $W \approx 1$. Thus, the viscous instability ceases to exist for $W \gg 1$. However, for $\beta < 0.5$, which represents the concentrated polymeric solutions and the polymer melts and also includes the case of a Maxwell fluid ($\beta=0$), the shortwave instability is found to persist even in the high Weissenberg number limit. As the shortwave instability is an interfacial mode (the eigenfunctions are confined to a region of thickness comparable to the disturbance wavelength near the fluid-solid interface), the value of Γ_c for this mode is independent of solid thickness H . Figure 4(b) shows the effect of the Weissenberg number on the critical shear rate Γ_c for thick solids with $H=10$ and 100. For this case, the critical mode of instability in the Newtonian limit ($W \rightarrow 0$) is the finite wavenumber mode. The Weissenberg number is found to have a stabilizing influence on this mode, as Γ_c increases with W , and there exists W_{\max} such that for any Weissenberg number $W > W_{\max}$, the finite wavenumber instability ceases to exist. W_{\max} is found to increase proportional to H . However, for $\beta < 0.5$, the shortwave instability

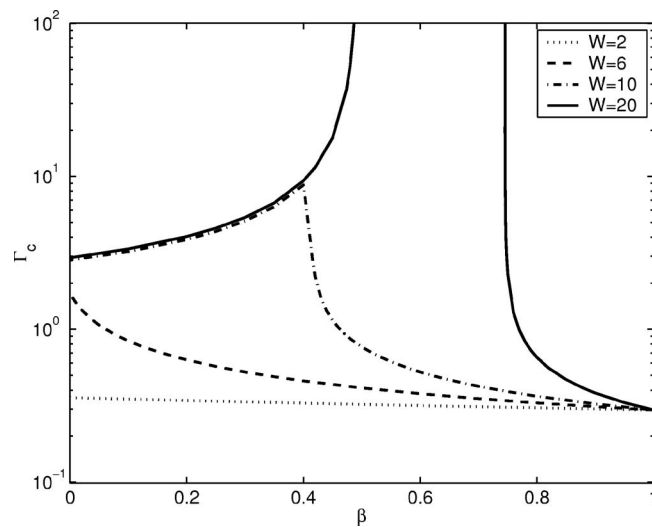


FIG. 5. Effect of β on the critical shear rate Γ_c for $H=10$, $\eta_r=0$, and $T=0$.

exists for high Weissenberg number as shown in Fig. 4(a), hence the critical mode crosses from the finite wavenumber mode to the shortwave mode at $W=W_{\max}$, as indicated by the plateau in Γ_c for a high Weissenberg number. For $\beta \geq 0.5$, the shortwave instability is absent in the high Weissenberg limit, and hence the flow becomes stable for $W > W_{\max}$, where $W_{\max} \propto H$.

The above discussed results are now presented in terms of various parameters in order to provide a comprehensive picture of the stability boundaries in different parameter domains. Figure 5 shows Γ_c against β for $H=10$ and different values of W . Beginning with the Newtonian viscous mode ($\beta=1$), the effect of polymer addition, reflected by reducing β , is found to be stabilizing, resulting in an increase in Γ_c . The shortwave instability that is present for $\beta < 0.5$ becomes critical in the limit of large Weissenberg number ($W/H \geq 1$), and an increase in β results in an increase in Γ_c for the shortwave mode. Thus, the solvent viscosity has a stabilizing influence on the upstream traveling shortwave mode of instability. Figure 5 further shows that for the high Weissenberg number flow, the shortwave instability is absent for the dilute polymeric solutions, as Γ_c for this mode diverges as β approaches the value of 0.5. The variation of Γ_c with solid thickness H is shown in Fig. 6 for $\beta=0.5$ and different values of W . The plateau in Γ_c for $H < 1$ and $W \leq 1$ indicates the shortwave mode. For the finite wavenumber mode, which is critical for the thick solids, Γ_c is shown to decrease proportional to H^{-1} for $H \geq 1$. The scalings of Γ_c and Weissenberg number with H are shown in Fig. 7, where Γ_c vs W is plotted for $\beta=0.8$ and $H \geq 10$. The results for different values of H are shown to collapse onto a single curve in the limit $H \geq 1$, when $\Gamma_c H$ is plotted against the scaled Weissenberg number W/H . This figure further establishes that the Weissenberg number W_{\max} beyond which the finite wavenumber instability ceases to exist scales with H for $H \geq 1$. This finding for the dilute polymer solutions is similar to the behavior of the UCM fluid past a linear viscoelastic solid.¹⁶

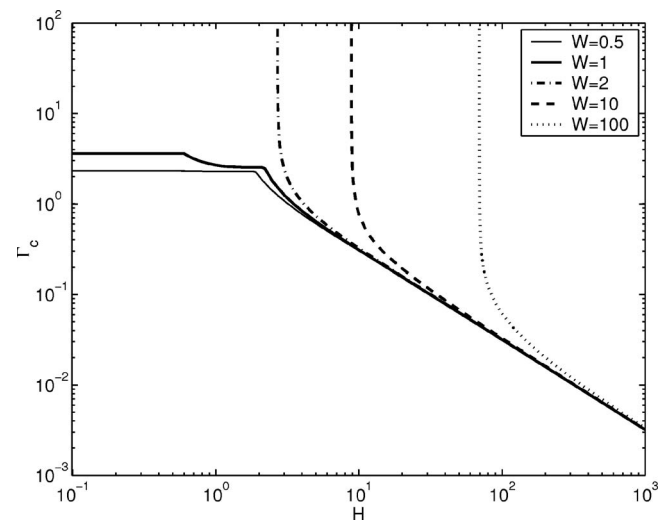


FIG. 6. Effect of wall thickness H on the critical shear rate Γ_c for $\beta=0.5$, $\eta_r=0$, and $T=0$. The plateau in Γ_c for thin solids represents the shortwave instability.

Since interfacial tension is known to eliminate the shortwave instability,^{8,14} the role of interfacial tension T was examined. For the finite wavenumber mode, the interfacial tension tends to increase Γ_c , indicating the stabilizing influence of T . However, we observe that the interfacial tension as high as $T=1000$ does not affect Γ_c for the shortwave instability to a considerable extent, and the plateau in Γ_c for $W \geq 1$ remains unchanged upon introducing the interfacial tension.

To summarize the stability behavior, we construct a plot in parametric space specifying the regions where the finite wavenumber instability and the shortwave instability are predicted. Figure 8 indicates the instability regions in the parametric space W/H - β for $H \geq 1$ and $\eta_r=0$. For a small Weissenberg number ($W/H < 1$), the finite wavenumber instability is present for all values of β . As mentioned earlier, Γ_c for this mode increases with W and diverges at $W/H \approx 1$,

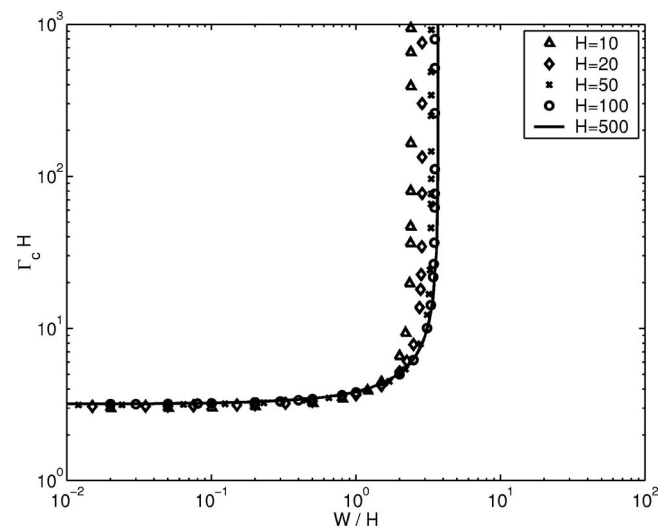


FIG. 7. $\Gamma_c H$ as a function of the scaled Weissenberg number W/H for $\beta=0.8$, $\eta_r=0$, and $T=0$. The data for different values of H fall on a single curve in the limit $H \geq 1$.

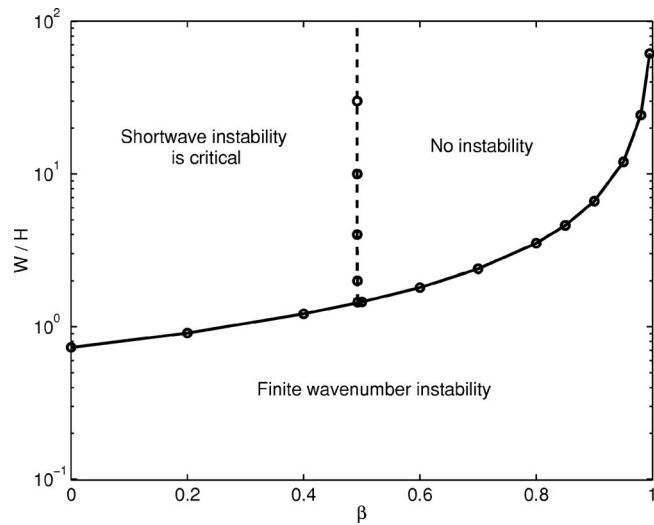


FIG. 8. Stability behavior in the parametric space W/H - β for $\eta_r=0$ and $T=0$. This plot holds for $H \gg 1$. For any point along the solid line, Γ_c for the finite wavenumber mode diverges as W is increased, and for any point along the broken line, Γ_c for the shortwave mode diverges as β is increased.

leading to the disappearance of finite wavenumber instability for $W \gg 1$. In the limit of high Weissenberg number, the shortwave instability is, however, present for $\beta < 0.5$. As Γ_c for the shortwave mode diverges as β approaches the value of 0.5, there is no instability in the high Weissenberg limit in the region of $0.5 \leq \beta < 1$, representing the dilute polymer solutions.

Finally, we comment on the typical parameter values of relevance to recent experiments.^{11,12,21} The shear modulus G of the aqueous polymer gels used in these experiments was estimated to be around 1000–5000 N/m². The viscosity of the Newtonian fluid used in the experiments was $\eta \approx 1$ N s/m². However, the viscosity of a polymeric fluid is around $\eta \approx 10$ –100 N s/m² and the relaxation time λ is anywhere between 0.001 and 0.1 s, depending on the concentration of the polymer chains. For these estimates, the Weissenberg number can be in the range 0.01–50. The present analysis covers this experimentally feasible parameter regime in which both the finite wavenumber mode and the shortwave mode of instability may be observed depending upon the value of solid-to-fluid thickness ratio H and polymer concentration parameter β . The gel viscosity can be estimated as $\eta_g \approx 10^3$ N s/m², which means the relative viscosity η_r is around 10–100. Therefore, the viscous stresses in the solid medium need to be taken into consideration. The influence of η_r on the instability will be discussed later.

2. Comparison with the linear elastic solid

The linear stability of the flow of an Oldroyd-B fluid past a linear viscoelastic solid was analyzed by Chokshi and Kumaran¹⁷ and the results of that analysis are seemingly in contradiction with the present results. We analyze this difference in detail before proceeding to the weakly nonlinear analysis. Figure 9 shows the regions of critical stability in W/H - β space for $H \gg 1$ constructed using the linear elastic constitutive model. As for the neo-Hookean solid, the insta-

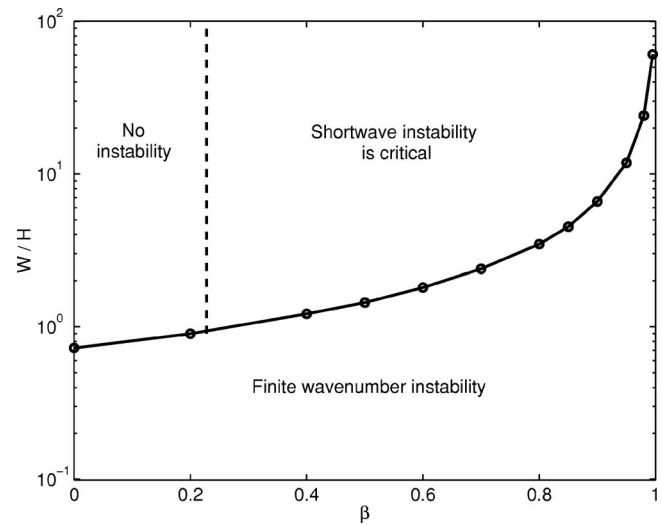


FIG. 9. Stability behavior for the linear elastic solid for $H \gg 1$.

bility is excited by the finite wavenumber mode for $W/H \leq 1$. Since the additional finite deformation terms in the neo-Hookean model are proportional to the base-state strain in the solid, and Γ_c is known to scale as $1/H$ for $H \gg 1$,^{3,16} the behavior of the finite wavenumber mode is similar for both models for $H \gg 1$. The striking difference, however, is the behavior of the shortwave instability. The range of β for which the shortwave mode is unstable is $0.23 \leq \beta < 1$ for the linear elastic solid,¹⁷ whereas it is $0 \leq \beta < 0.5$ for the neo-Hookean solid. To investigate further, we carry out an asymptotic analysis of the shortwave disturbance mode.

In the shortwave asymptotic analysis, the characteristic length scale is the inverse of the wavenumber, $\delta = 1/\alpha$, for wavenumber $\alpha \gg 1$. Keeping $\Gamma \sim W \sim O(1)$, the cross-stream distance from the interface, and the wavespeed, are scaled by δ . The leading-order fluid velocity and solid displacement eigenfunctions are $O(1)$ and the stresses are $O(1/\delta)$. The leading-order governing equations for the solid can be solved analytically for both the linear and neo-Hookean elastic models. In the fluid side, the governing equations admit analytical solutions for the case of UCM fluid, that is, for $\beta = 0$.¹⁶ After imposing the interface conditions on the solutions, we obtain the leading-order complex wavespeed c as the eigenvalue. Table I shows the wavespeed c from the asymptotic analysis and compares them with the numerically obtained wavespeed for wavenumber $\alpha = 10$ for both models. Note that in addition to the discrete modes, there is a continuous spectrum of eigenvalues that remains stable for all values of Weissenberg number and β . For $\beta = 0$, one of the three discrete modes is unstable ($c_i > 0$) for the neo-Hookean solid, whereas all the discrete modes are stable for the linear elastic solid. Thus, the normal-stress difference arising due to finite deformations in the neo-Hookean model drives an instability; this normal-stress difference is absent for the linear elastic solid, which is stable. The jump in the normal-stress difference across the interface excites a shortwave instability in the Newtonian flow.⁸ The shortwave instability for the polymeric fluid is the continuation of the instability in the Newtonian flow [refer to Fig. 4(a)]. Like the Newtonian

TABLE I. Complex wavespeed c estimated from the shortwave asymptotic analysis carried out for the neo-Hookean as well as the linear elastic solid for different values of β . The asymptotic value is compared with the numerically calculated c .

Neo-Hookean solid: $W=1, \Gamma=3, \alpha=10$		
	Shortwave asymptotic	Numerical
$\beta=0$	$-0.0528333+0.0119862i$	$0.052833328+0.011986242i$
	$0.0402700-0.0297675i$	$0.040269972-0.029767540i$
	$0.0599975-0.1537430i$	$0.059997521-0.153743009i$
$\beta=0.2$	$-0.0576291+0.0076315i$	$-0.057629096+0.007631493i$
$\beta=0.4$	$-0.0637346+0.0018509i$	$-0.063734611+0.001850861i$
$\beta=0.6$	$-0.0722768-0.0054382i$	$-0.072276774-0.005438176i$
$\beta=0.8$	$-0.0875634-0.1238660i$	$-0.087563381-0.12386588i$
Linear elastic solid: $W=1, \Gamma=10, \alpha=10$		
	Shortwave asymptotic	Numerical
$\beta=0$	$-0.0088985-0.0015213i$	$-0.008898477-0.001521282i$
	$0.0498296-0.0178490i$	$0.049829608-0.017849025i$
	$0.0502094-0.1797640i$	$0.050209385-0.179763832i$
$\beta=0.2$	$0.0555289-0.0101962i$	$0.055528908-0.010196195i$
$\beta=0.4$	$0.0608055+0.0009938i$	$0.060805535+0.000993846i$
$\beta=0.6$	$0.0636685+0.0135064i$	$0.063668536+0.013506351i$
$\beta=0.8$	$0.0709075+0.0232392i$	$0.070907512+0.023239215i$

fluid, the unstable shortwave mode for the viscoelastic fluid is an upstream traveling disturbance, as indicated by the negative sign of the real part of the wavespeed.

For $\beta > 0$, the fluid eigenfunctions are in the form of hypergeometric functions and the eigenvalues are obtained numerically by an iterative procedure starting with an initial guess value. The variation with β of the growth rate of the unstable mode is shown in Table I for both models. The leading-order value of c is found to be in good agreement with the numerically calculated wavespeed for $\alpha=10$. Referring to the three eigenvalues listed for $\beta=0$ as mode 1, 2, and 3 in the order of listing, the variation of c_i for mode 1 and mode 2 with β is plotted in Fig. 10. It should be noted that mode 1 is an upstream traveling wave, while mode 2 is a downstream traveling disturbance. As shown in Fig. 10(a), the shortwave instability in the neo-Hookean solid is an upstream traveling mode and the instability is present for $\beta < 0.5$. For β close to 1, c_i becomes positive, as the shortwave mode is known to be unstable for the Newtonian fluid ($\beta=1$). Interestingly, for the linear elastic solid, the upstream traveling mode (that is, mode 1) remains stable for all values of β , as shown in Fig. 10(b). However, mode 2, which is the downstream traveling mode, becomes unstable as β increases beyond 0.4 for $\Gamma=10$. For Γ larger than 10, the instability appears for β as low as 0.23.¹⁷ Thus, while the instability in both of the solids is of a shortwave nature, there are subtle differences between them. The one for the neo-Hookean solid is an upstream traveling wave and is understood to arise due to the normal-stress difference in the solid, which is why this instability is qualitatively similar to the one observed in the Newtonian flow past a neo-Hookean solid. On the other hand, the instability for the linear elastic

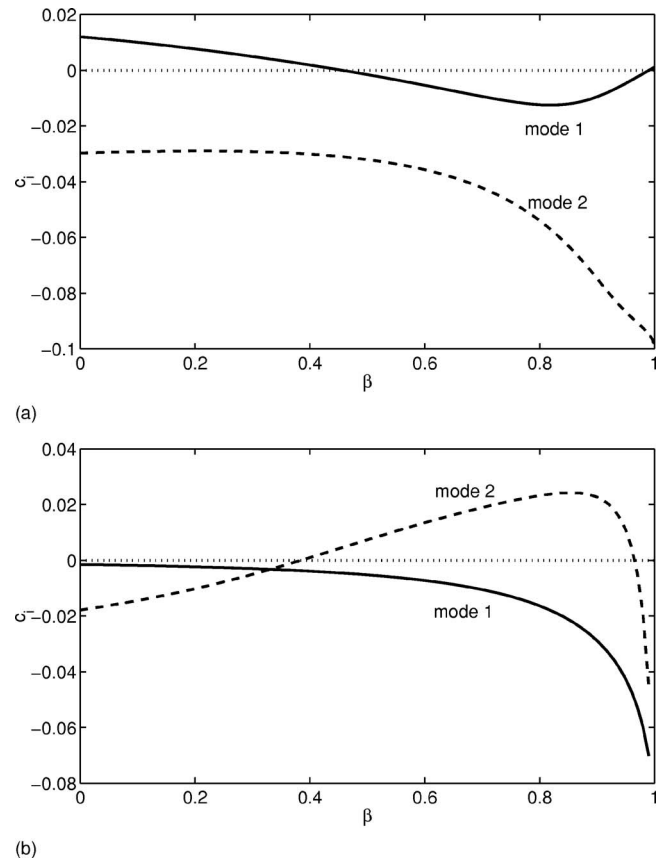


FIG. 10. Variation of the imaginary part of c for the first two discrete modes with β for $W=1$ and $\alpha=10$. (a) Neo-Hookean elastic solid with shear rate $\Gamma=3$; (b) linear elastic solid with $\Gamma=10$.

solid is a downstream traveling wave and is absent for the flow of Newtonian fluids. As this instability does not continue in the limit $W \rightarrow 0$, it is referred to in Ref. 17 as the highly elastic instability.

3. Effect of solid viscosity

Having studied the influence of W , β , and H on Γ_c for a nondissipating elastic medium, we now analyze the effect of solid viscosity on Γ_c . The viscous stresses are modeled using a Maxwell-type equation (20) with Deborah number De as the dimensionless relaxation time in the solid. Figure 11 plots $\Gamma_c H$ against the scaled parameter $\sqrt{\eta_r}/H$ for $H=10$ and $W=10$. While the results are plotted for $De=10$, it should be noted here that the plot does not change significantly for $De=0-20$. For Deborah number larger than 20, the numerical value of Γ_c varies, but the qualitative nature of the graph remains unchanged. For a Newtonian fluid ($\beta=1$), the linear viscoelastic solid analyzed by Ref. 3 predicts that the instability ceases to exist for $\sqrt{\eta_r}/H > 1$. However, as shown in Fig. 11, the unstable traveling waves exist even for $\sqrt{\eta_r}/H > 1$ for the neo-Hookean solid. Interestingly, an increase in η_r is found to cause contrasting variations in Γ_c in the ranges $\sqrt{\eta_r}/H < 1$ and $\sqrt{\eta_r}/H > 1$. While increasing η_r has a stabilizing influence on Γ_c in the regime $\sqrt{\eta_r}/H < 1$, the influence is destabilizing (as increase in η_r tends to reduce Γ_c) in the regime $\sqrt{\eta_r}/H > 1$. This opposing effect of η_r is specific to

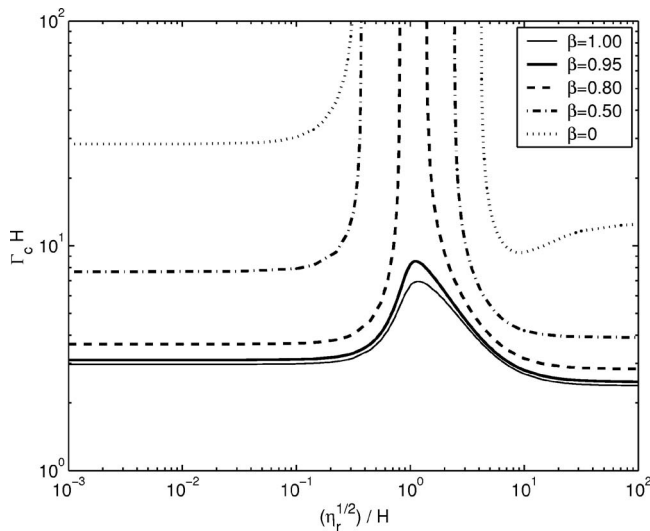


FIG. 11. Effect of η_r on Γ_c plotted on the scaled coordinates $\Gamma_c H$ vs $\sqrt{\eta_r}/H$ for $H=10$, $W=10$, $De=10$, $T=0$, and different values of β . The gray shaded curve represents the Newtonian fluid. The curve for $\beta=0$ (UCM fluid) depicts the shortwave mode.

the neo-Hookean expression of the strain rate tensor (22), since it is not present in the linear viscoelastic model. The peak value of Γ_c at $\sqrt{\eta_r}/H=1$ increases upon introducing the polymer chains in the solvent. For $\beta \leq 0.8$, there exists a stable region around $\sqrt{\eta_r}/H=1$ that widens upon decreasing β .

B. Weakly nonlinear stability analysis

Following the procedure outlined in Sec. III, the first Landau constant $s_r^{(1)}$ is calculated at the critical point (α_c, Γ_c) . For the Newtonian fluid ($W \rightarrow 0$), the sign of $s_r^{(1)}$ is found to be positive, indicating that the bifurcation is subcritical. This observation is consistent with the earlier finding of Shankar and Kumaran,²⁰ who, using the linear viscoelastic solid, reported that $s_r^{(1)}$ is always positive for a wide range of parameters H and η_r . As the fluid elasticity is increased, the value of $s_r^{(1)}$ is found to decrease. The bifurcation, however, remains subcritical for the polymeric viscous mode. A quantity of interest in a nonlinear stability analysis is the equilibrium amplitude A_{1e} . For a subcritical instability, the system is unstable to finite-amplitude disturbances even when the strain rate is below the critical value Γ_c , and the equilibrium amplitude is the minimum amplitude required to render the system unstable for $\Gamma < \Gamma_c$. The equilibrium amplitude, obtained by setting $dA/d\tau=0$ in the scaled Landau equation (36), is given as

$$A_{1e}^2 = \frac{(ds_r^{(0)}/d\Gamma)(\Gamma_c - \Gamma)}{s_r^{(1)}}. \quad (37)$$

It is important to note that the numerical values of the Landau constant, and hence the values of A_{1e}^2 , depend upon the normalization condition used to obtain the eigenfunctions of the linear stability problem. In the present study, the normalization condition $\tilde{v}_y^{(1,1)} = (1+i)$ at $y=0$ has been used.

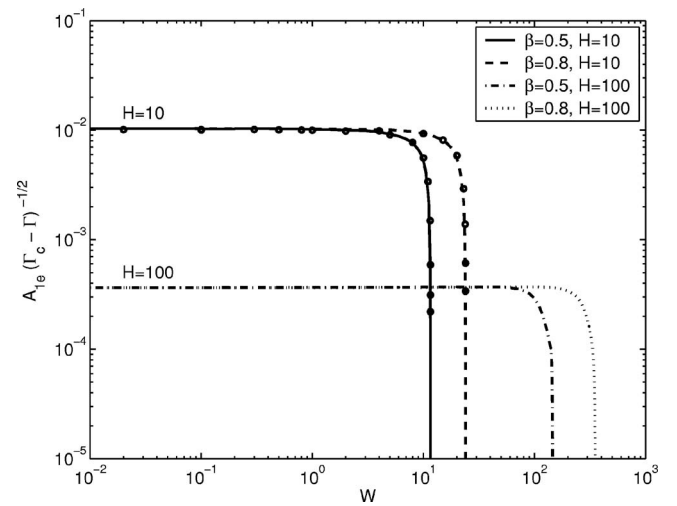


FIG. 12. Variation of the equilibrium amplitude $A_{1e}/\sqrt{(\Gamma_c - \Gamma)^{-1/2}}$ with Weissenberg number for $H=10$ and 100 . η_r and T are kept zero. The symbols on plots for $H=10$ are explained in the Discussion section.

The variation of the equilibrium amplitude with Weissenberg number is shown in Fig. 12 for $H=10$ and 100 and $\beta=0.5$ and 0.8 , for which the system goes unstable due to the finite wavenumber instability. The equilibrium amplitude is nearly a constant for low W , but it decreases sharply at W_{\max} , beyond which the linear stability analysis predicts that the perturbations are always stable. The small symbols on the plots for $H=10$ indicate the equilibrium amplitude, $A_{1e}/\sqrt{(\Gamma_c - \Gamma)^{-1/2}}$, estimated from the unscaled Landau equation (35) wherein the actual linear growth rate $s_r^{(0)}$ is used instead of expanding it as $(\Gamma - \Gamma_c)(ds_r^{(0)}/d\Gamma)|_{\Gamma=\Gamma_c}$. For this, the equilibrium amplitude is calculated at shear rate $(\Gamma_c - \Gamma)/\Gamma_c = 0.1$. As discussed in Sec. IV A 1, W_{\max} increases proportional to H for $H \gg 1$. In this limit, the equilibrium amplitude $A_{1e}/\sqrt{(\Gamma_c - \Gamma)^{-1/2}}$ is found to decrease proportional to $H^{-3/2}$.

Next, we analyze the shortwave mode, which, for the case $H \gg 1$, becomes the most unstable mode for $\beta < 0.5$ and $W/H \gg 1$. We mentioned earlier that the critical shear rate Γ_c does not show much variation as the interfacial tension T is increased, but the critical wavenumber α_c is significantly reduced for nonzero T . As the eigenfunctions for the shortwave mode for $T=0$ are confined to a very thin layer of thickness $O(1/\alpha_c)$ near the fluid-solid interface, the numerical scheme used in the present study does not work satisfactorily when $\alpha_c \gg 1$, especially for the case $W \gg 1$. Because of the numerical issues and the fact that the interfacial tension is nonzero in a real system, we consider a nonzero value of T to analyze the shortwave instability in the limit of high Weissenberg number. The value of $s_r^{(1)}$ for the shortwave modes is found to be very large. Thus, the linear instability is highly subcritical. Figure 13 shows the variation of the equilibrium amplitude with the fluid Weissenberg number for the upper convected Maxwell fluid. For $W \leq 6$, the instability is driven by the finite wavenumber mode and for $W > 6$, the only mode of instability present is the shortwave mode. For the former class of instability, the equilibrium amplitude decreases sharply at $W \approx 6$, and for the latter mode, the amplitude decreases proportional to W^{-2} for $W > 6$. As the numerical

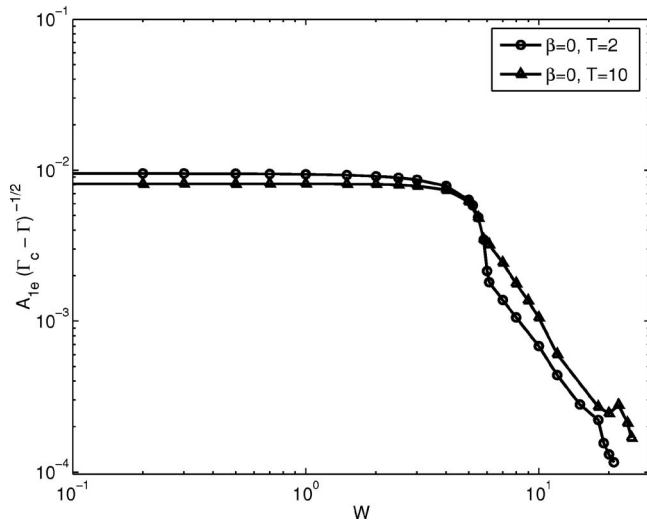


FIG. 13. Variation of the equilibrium amplitude $A_{1e}/\sqrt{(\Gamma_c-\Gamma)}$ with Weissenberg number for $H=10$ and $\beta=0$. η_r is kept zero.

scheme fails for the shortwave instability in the limit $W \gg 1$, the calculations were possible only up to $W/H \approx 3$. A similar plot showing the equilibrium amplitude as a function of the fluid elasticity for thin solids is shown in Fig. 14 for $H=1$ and $T=1$.

Another quantity of interest is the energy of perturbations due to the deformation of the solid, which is independent of the normalization scheme employed. The rate of work done at the fluid-solid interface, which is given by the expression $\int_{\mathcal{A}} (\mathbf{n} \cdot \boldsymbol{\tau} \cdot \mathbf{v} + \mathbf{n} \cdot \boldsymbol{\sigma} \cdot \mathbf{v}^g) dA$, where \mathcal{A} is the surface area of the interface, is the power input to the disturbance energy. In general, a part of this deformation work is dissipated in the fluid and the solid domain, while the remaining is stored as the elastic energy of deformation and the kinetic energy of the fluid.⁴ For the flow in the limit of zero Rey-

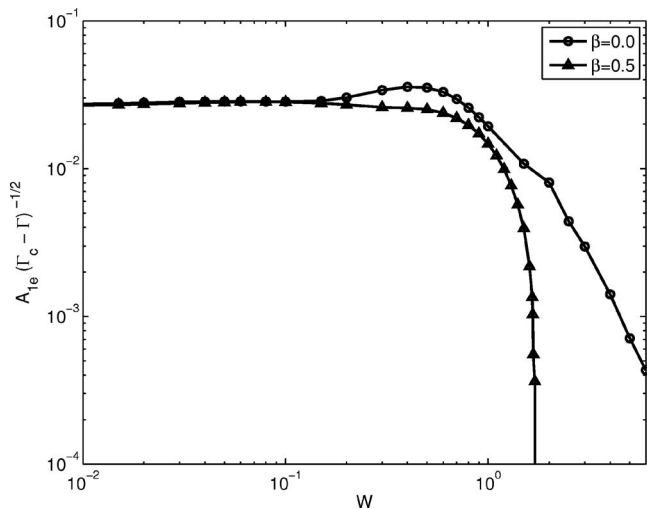


FIG. 14. Variation of the equilibrium amplitude $A_{1e}/\sqrt{(\Gamma_c-\Gamma)}$ with Weissenberg number for $H=1$, $T=1$, and $\eta_r=0$. As $H < 1.2$, the instability is excited by the shortwave mode for all values of Weissenberg number.

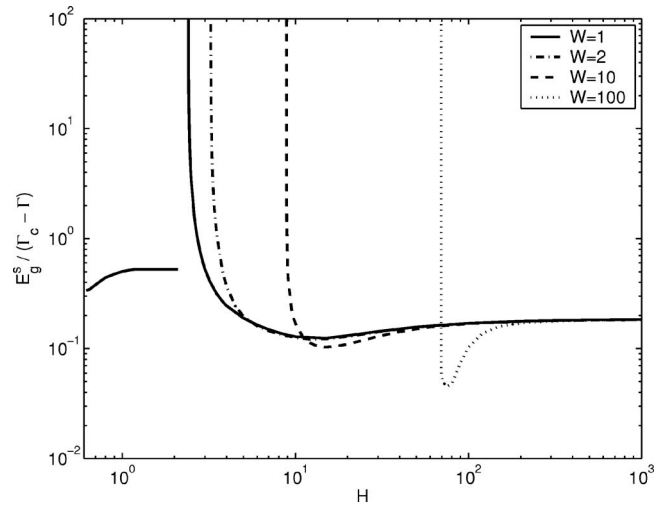


FIG. 15. Variation of the threshold strain energy for the elastic solid, $E_g^s/(\Gamma_c-\Gamma)$, with solid thickness H for $\beta=0.5$, $\eta_r=0$, and $T=0$.

nolds number, the disturbance kinetic energy is small compared to the elastic energy of deformation, which is defined as

$$E_g^s = \frac{A_{1e}^2}{2} \int_{-H}^0 \tilde{\boldsymbol{\sigma}}_e^{(1,1)} \tilde{\mathbf{e}}^{(1,1)} dy. \quad (38)$$

For a subcritical instability, this energy represents the threshold energy required for destabilizing the system when the strain rate is below the transition value. Figure 15 provides the threshold strain energy in the form $E_g^s/(\Gamma_c-\Gamma)$ as a function of the solid thickness H for $\beta=0.5$ and $T=0$. It was shown in Sec. IV A 1 that for $\beta=0.5$ and $W \leq 1$, the instability is excited by the shortwave mode for thin solids with $H < 2$ and the finite wavenumber mode for thick solids with $H \gg 1$ (refer to Fig. 6). The threshold energy for both of these modes is shown in Fig. 15. The discontinuity in the plots for $W=1$ is due to the crossover from the shortwave mode being critical to the finite wavenumber instability being critical. For $W > 1$, the shortwave instability is absent and the threshold energy for the finite wavenumber mode, which is an $O(1)$ quantity, diverges as the shear rate Γ_c diverges.

Next, we analyze the effect of viscosity of the solid on the nature of the bifurcation, and find that an increase in viscosity in the solid changes the nature of the bifurcation from subcritical to supercritical. For the supercritical bifurcation, the Landau constant $s_r^{(1)}$ is negative, and a perturbation that is unstable in the linear analysis saturates to a value

$$A_{1e}^2 = \frac{(ds_r^{(0)}/d\Gamma)(\Gamma - \Gamma_c)}{|s_r^{(1)}|} \quad (39)$$

for $\Gamma > \Gamma_c$. The effect of η_r , the solid-to-fluid viscosity ratio, on the finite-amplitude instability is presented in Fig. 16, where the threshold strain energy is plotted against $\sqrt{\eta_r}/H$ for the case $H=10$, $W=10$, and $De=10$. Here, solid lines represent the energy $E_g^s/(\Gamma_c-\Gamma)$ for the subcritical instability, and the broken lines show the energy $E_g^s/(\Gamma-\Gamma_c)$ when the bifurcation is supercritical. It has been shown in the linear stability analysis (refer to Fig. 11) that there are two

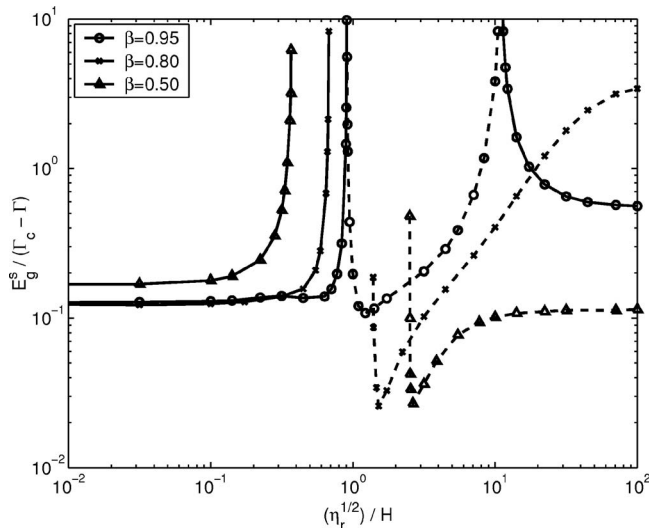


FIG. 16. Effect of η_r in the form $\sqrt{\eta_r}/H$ on the total strain energy for the solid for $H=10$, $W=10$, $De=10$, and $T=0$. $E_g^s/(\Gamma_c-\Gamma)$ is positive for the subcritical bifurcation and is negative for the supercritical bifurcation. For the latter case, $E_g^s/(\Gamma-\Gamma_c)$ is plotted as broken lines. Thus, the broken lines indicate the supercritical stability.

regimes where the effect of solid viscosity is qualitatively different: for small $\sqrt{\eta_r}/H$, the solid viscosity stabilizes perturbations, while for large $\sqrt{\eta_r}/H$, perturbations are destabilized by an increase in solid viscosity. The present nonlinear analysis reveals that, correspondingly, the bifurcation for $\sqrt{\eta_r}/H < 1$ is subcritical, whereas that for $\sqrt{\eta_r}/H > 1$ is supercritical. For very dilute polymeric solutions with $\beta=0.95$, the supercritical stability is limited only in a narrow band of $\sqrt{\eta_r}/H \approx 1-10$, whereas the bifurcation is subcritical for very large $\sqrt{\eta_r}/H$.

It is of practical interest to determine the reduction in the critical shear rate from its value predicted by the linear theory (Γ_c) for the subcritical bifurcation, due to finite-amplitude nature of the disturbances. We take the normal displacement of the fluid-wall interface as the representative quantity for the disturbance amplitude. The normal displacement of the interface, correct to $O(\epsilon)$, is given by

$$|u'_y|_{y=0} = A_1 \epsilon |\tilde{u}_y^{(1,1)}|_{y=0}. \quad (40)$$

Table II provides the percentage reduction in Γ from Γ_c for different levels of normal displacement of the interface. For $H=1$, where the shortwave mode is the most unstable, the reduction in critical shear rate is significant, as the finite-amplitude nonlinear effects are strongly destabilizing. Hence, for a given level of disturbance, the shortwave instability can be observed at a shear rate significantly smaller than its value predicted by the linear stability. However, for the remaining set of parameters, where the finite wavenumber mode is the most unstable, the reduction in Γ_c is about 10% for a disturbance of magnitude 0.1. For this case, the finite-amplitude disturbances do not result in a significant reduction in the critical shear rate from the predictions of the linear stability theory.

TABLE II. Reduction in the critical velocity Γ required for instability when the flow is subcritical. Here Γ_c is the critical velocity obtained from the linear stability analysis and Γ is the critical velocity for the finite-amplitude disturbance. Here, the normal displacement of the interface is taken as the representative of the perturbation amplitude.

	β	W	T	Interface displacement amplitude, $ u'_y _{y=0}$	% reduction in Γ ($(\Gamma_c-\Gamma)/\Gamma_c \times 100$)
$H=1$	0	1	1	0.010	1.408
	0	1	1	0.100	140.85
	0.2	1	0	0.010	2.937
	0.2	1	0	0.025	18.354
	0.2	1	0	0.100	293.66
	0.5	1	0	0.025	23.967
$H=10$	0.5	1	0	0.100	383.47
	0	5	0	0.025	0.722
	0	5	0	0.100	11.559
	0.5	10	0	0.025	0.825
	0.5	10	0	0.100	13.201
	0.8	20	0	0.025	0.718
$H=100$	0.8	20	0	0.100	11.492
	0	50	0	0.025	0.769
	0	50	0	0.100	12.299
	0.8	200	0	0.050	2.257
	0.8	200	0	0.100	9.026

V. CONCLUSIONS

The stability of a plane shear flow of a viscoelastic fluid in the limit of creeping flow past an incompressible neo-Hookean solid was studied using both the linear and weakly nonlinear stability analyses. The viscoelastic fluid is described by an Oldroyd-B model. The previous analysis for the Newtonian fluid past a neo-Hookean solid had observed two classes of instability modes: the shortwave instability, which is due to the jump in the first normal-stress difference across the fluid-solid interface and is the most unstable mode for thin solids ($H < 1.2$), and the finite wavenumber instability, which is the most unstable mode for relatively thick solids ($H > 1.2$).⁸ In the present study, the effect of fluid elasticity on both classes of modes is studied. The fluid Weissenberg number has a stabilizing influence on both kinds of modes, as it tends to increase the critical shear rate Γ_c , thus delaying the onset of instability. The stability behavior for the highly elastic fluid with $W/H > 1$ is found to depend upon the parameter β , which represents the influence of polymer chains on solution viscosity. For $\beta > 0.5$, which represents the dilute polymeric solutions, the viscous instability ceases to exist beyond a certain Weissenberg number W_{\max} , which increases proportional to H . For $\beta < 0.5$, which includes the special case of upper convected Maxwell fluid ($\beta=0$) and represents the case of concentrated polymeric solutions and the polymer melts, the shortwave instability is present in the limit $W \gg 1$. The highly elastic shortwave instability results in a plateau in Γ_c for $W \gg 1$. The viscous effects in the solid are also taken into account by supplementing the neo-Hookean elastic model with the viscous stresses modeled using a Maxwell-type equation. Using this augmented neo-Hookean viscoelastic model, the effect of

relative viscosity of the elastic medium η_r , on the stability is analyzed. The influence of η_r on critical shear rate Γ_c is stabilizing in the regime $\sqrt{\eta_r}/H < 1$, whereas for $\sqrt{\eta_r}/H > 1$, an increase in η_r tends to decrease Γ_c , indicating a destabilizing influence of the solid viscosity.

The weakly nonlinear analysis was carried out at the critical point (α_c, Γ_c) to investigate the role of the nonlinearities present in the governing equations and the matching conditions at the deformed interface. The first Landau constant $s^{(1)}$, whose real part provides the nonlinear correction to the linear growth rate, was calculated for a range of parameters. For a neo-Hookean elastic solid, the real part $s_r^{(1)}$ was found to be positive for both classes of instability modes, indicating a subcritical bifurcation. By balancing the linear damping and nonlinear growth in the vicinity of $\Gamma = \Gamma_c$, we obtained the equilibrium disturbance amplitude A_{1e} , which is the threshold amplitude for the subcritical instability at shear rate $\Gamma < \Gamma_c$. For $\beta \geq 0.5$, when the instability ceases to exist at Weissenberg number W_{\max} , the amplitude in the form $A_{1e}/\sqrt{(\Gamma_c - \Gamma)}$ decreases sharply at $W = W_{\max}$ for both classes of modes, and it scales as $H^{-3/2}$ for $H \gg 1$. For $\beta < 0.5$, the equilibrium amplitude for the highly elastic shortwave instability decreases slowly with an increase in the Weissenberg number, following an approximate scaling of W^{-2} for $W/H > 1$. The subcritical nature of bifurcation for $\eta_r = 0$ changes to supercritical when the viscous effects in the solid are taken into account. For $\sqrt{\eta_r}/H > 1$, the instability bifurcates to a supercritically stable flow. In this regime, the bifurcation again changes to subcritical in the limit $\eta_r \gg 1$ for very dilute polymeric solutions ($\beta > 0.8$). However, for $\beta \leq 0.8$, the supercritical nature of nonlinear bifurcation persists for $\eta_r \gg 1$.

For the subcritically unstable flows, we also calculated the % reduction in Γ from its value Γ_c for the flow to be destabilized by a finite-amplitude disturbance. For the finite wavenumber instability, when the disturbance amplitude is 2.5% of the channel width R , the reduction in the critical shear rate is very small, up to about 1%. However, for the shortwave mode of instability, the reduction in Γ for $W = 1$ is about 20% for the same level of disturbance amplitude, indicating a strong destabilizing influence of the nonlinearities on the shortwave instability.

There are two important conclusions from the present analysis. The first is that the nature of the instability is sensitive to the details of the wall model used, and the results for the neo-Hookean wall model are different from those for a linear elastic wall model. In the case of a Newtonian fluid, the flow past a neo-Hookean solid has an additional shortwave instability due to the first normal-stress difference, as first reported by Gkanis and Kumar,⁸ and this could become the most unstable mode for thin solids. However, for viscoelastic modes, we find that the effect of the Weissenberg number and the polymer concentration parameter β is very different for the linear and the neo-Hookean solid, and it is necessary to use the correct solid model in order to be able to predict the stability characteristics. The other important conclusion is that the dissipation in the solid has a complicated and nonintuitive effect on the stability characteristics. The solid viscosity is stabilizing, as expected, in the limit of

small $\sqrt{\eta_r}/H$, but it is destabilizing in the limit of large $\sqrt{\eta_r}/H$. The nature of the bifurcation is also significantly affected by dissipation in the solid: whereas the bifurcation is subcritical for small $\sqrt{\eta_r}/H$, it is supercritical for large $\sqrt{\eta_r}/H$. An accurate description of the dissipation in the solid is, therefore, necessary for quantitatively predicting the stability limits.

- ¹M. O. Kramer, "Boundary-layer stabilisation by distributed damping," *J. Aeronaut. Sci.* **24**, 458 (1957).
- ²P. Krindel and A. Silberberg, "Flow through gel-walled tubes," *J. Colloid Interface Sci.* **71**, 39 (1979).
- ³V. Kumaran, G. H. Fredrickson, and P. Pincus, "Flow induced instability of the interface between a fluid and a gel at low Reynolds number," *J. Phys. II* **4**, 893 (1994).
- ⁴V. Kumaran, "Stability of the viscous flow of a fluid through a flexible tube," *J. Fluid Mech.* **294**, 259 (1995).
- ⁵V. Kumaran, "Stability of an inviscid flow through a flexible tube," *J. Fluid Mech.* **320**, 1 (1996).
- ⁶V. Kumaran, "Stability of fluid flow through a flexible tube at intermediate Reynolds number," *J. Fluid Mech.* **357**, 123 (1998).
- ⁷V. Kumaran, "Stability of wall modes in a flexible tube," *J. Fluid Mech.* **362**, 1 (1998).
- ⁸V. Gkanis and S. Kumar, "Instability of creeping Couette flow past a neo-Hookean solid," *Phys. Fluids* **15**, 2864 (2003).
- ⁹L. E. Malvern, *Introduction to the Mechanics of a Continuous Medium* (Prentice-Hall, Englewood Cliffs, NJ, 1969).
- ¹⁰V. Gkanis and S. Kumar, "Stability of pressure-driven creeping flows in channels lined with a nonlinear elastic solid," *J. Fluid Mech.* **524**, 357 (2005).
- ¹¹V. Kumaran and R. Muralikrishnan, "Spontaneous growth of fluctuations in the viscous flow of a fluid past a soft interface," *Phys. Rev. Lett.* **84**, 3310 (2000).
- ¹²R. Muralikrishnan and V. Kumaran, "Experimental study of the instability of the viscous flow past a flexible surface," *Phys. Fluids* **14**, 775 (2002).
- ¹³V. A. Gorodtsov and A. I. Leonov, "On a linear instability of a plane parallel Couette flow of viscoelastic fluid," *J. Appl. Math. Mech.* **31**, 310 (1967).
- ¹⁴Y. Renardy, "Stability of the interface in two-layer Couette flow of the upper convected Maxwell liquids," *J. Non-Newtonian Fluid Mech.* **28**, 99 (1988).
- ¹⁵H. J. Wilson, M. Renardy, and Y. Renardy, "Structure of the spectrum in zero Reynolds number shear flow of the UCM and Oldroyd-B liquids," *J. Non-Newtonian Fluid Mech.* **80**, 251 (1999).
- ¹⁶V. Shankar and S. Kumar, "Instability of viscoelastic plane Couette flow past a deformable wall," *J. Non-Newtonian Fluid Mech.* **116**, 371 (2004).
- ¹⁷P. Chokshi and V. Kumaran, "Stability of the viscous flow of a polymeric fluid past a flexible surface," *Phys. Fluids* **19**, 034102 (2007).
- ¹⁸J. T. Stuart, "On the non-linear mechanics of wave disturbances in stable and unstable parallel flows. Part 1: The basic behavior in plane Poiseuille flow," *J. Fluid Mech.* **9**, 353 (1960).
- ¹⁹J. Watson, "On the non-linear mechanics of wave disturbances in stable and unstable parallel flows. Part 2: The development of a solution for plane Poiseuille and for plane Couette flow," *J. Fluid Mech.* **9**, 371 (1960).
- ²⁰V. Shankar and V. Kumaran, "Weakly nonlinear stability of viscous flow past a flexible surface," *J. Fluid Mech.* **434**, 337 (2001).
- ²¹M. D. Eggert and S. Kumar, "Observations of instability, hysteresis, and oscillation in low-Reynolds number flow past polymer gels," *J. Colloid Interface Sci.* **278**, 234 (2004).
- ²²N. Phan-Thien, "Squeezing flow of a viscoelastic solid," *J. Non-Newtonian Fluid Mech.* **95**, 343 (2000).
- ²³J. M. Rotenberry and P. G. Saffman, "Effect of compliant boundaries on weakly nonlinear shear waves in channel flow," *SIAM J. Appl. Math.* **50**, 361 (1990).
- ²⁴L. Srivatsan and V. Kumaran, "Flow induced instability of the interface between a fluid and a gel," *J. Phys. II* **7**, 947 (1997).
- ²⁵V. Shankar, "Linear and weakly nonlinear stability of fluid flow through flexible tubes and channels," Ph.D. thesis, Indian Institute of Science, Bangalore (2000).
- ²⁶R. M. Thaokar and V. Kumaran, "Stability of fluid flow past a membrane," *J. Fluid Mech.* **472**, 29 (2002).